Iron Oxide Nanoparticle - Multiwall Carbon Nanotube Composite Materials for Batch or Chromatographic Biomolecule Separation

Sebastian Patrick Schwaminger (s.schwaminger@tum.de)
Technical University of Munich: Technische Universitat Munchen https://orcid.org/0000-0002-8627-0807

Markus Brammen
Technical University of Munich: Technische Universitat Munchen

Florian Zunhammer
Technical University of Munich: Technische Universitat Munchen

Nicklas Däumler
Technical University of Munich

Paula Fraga-García
Technical University of Munich

Sonja Berensmeier
Technical University of Munich

Nano Express

Keywords: Iron oxides, Nanoparticles, Magnetic separation, Multiwall carbon nanotubes, Mixed-mode chromatography, Amino acids

Posted Date: December 9th, 2020

DOI: https://doi.org/10.21203/rs.3.rs-122143/v1

Version of Record: A version of this preprint was published on February 10th, 2021. See the published version at https://doi.org/10.1186/s11671-021-03491-5.

Iron oxide nanoparticle - multiwall carbon nanotube composite materials for batch or chromatographic biomolecule separation

Sebastian P. Schwaminger*, Markus W. Brammen, Florian Zunhammer, Nicklas Däumler, Paula Fraga-García, Sonja Berensmeier*

Bioseparation Engineering Group, Department of Mechanical Engineering, Technical University of Munich, Boltzmannstraße 15, 85748 Garching, Germany

Corresponding Author

*s.schwaminger@tum.de

*s.berensmeier@tum.de

Abstract: Carbon-based materials are the spearhead of research in multiple fields of nanotechnology. Moreover, their role as stationary phase in chromatography is gaining relevance. We investigate a hybrid material consisting of multiwall carbon nanotubes (CNTs) and superparamagnetic iron oxide nanoparticles (SPIONs) towards its use as a mixed-mode chromatography material. The idea is to immobilize the ion exchange material iron oxide on CNTs as a stable matrix for chromatography processes without a

significant pressure drop. Iron oxide nanoparticles are synthesized and used to decorate the CNTs via a co-precipitation route. They bind to the walls of oxidized CNTs, thereby enabling to magnetically separate the hybrid material. This hybrid material is investigated with transmission electron microscopy, magnetometry, X-ray diffraction, X-ray photoelectron and Raman spectroscopy. Moreover, we determine its specific surface area and its wetting behavior. We also demonstrate its applicability as chromatography material for amino acid retention, describing the adsorption and desorption of different amino acids in a complex porous system surrounded by aqueous media. Thus, this material can be used as chromatographic matrix and as a magnetic batch adsorbent material due to the iron oxide nanoparticles. Our work contributes to current research on composite materials. Such materials are necessary for developing novel industrial applications or improving the performance of established processes.

Keywords: Iron oxides, Nanoparticles, Magnetic separation, Multiwall carbon nanotubes, Mixed-mode chromatography, Amino acids

Introduction

Since the first synthesis of carbon nanotubes (CNTs) 1991 by Iijima [1] a matchless rise to one of the most powerful nanomaterials has begun. The production of CNT is based on the rolling of graphene layers to tubes. The electrical and mechanical properties of the CNTs can easily be tuned by different conformation of layers or multilayer assemblies. High elasticity, stability, thermal and electrical conductivity combined with a high specific surface area position CNTs to the spearhead of nanotechnology [2]. The applications of

CNTs range from battery, sensors and high performance materials to drug delivery and wastewater treatment [2–9]. Many applications are based on the unique sorption properties of CNTs which possess a high specific surface area and a defined chemical structure. Long and Yang observed a strong adsorption behavior of the gases dioxane and nitrogen oxide while sulfur oxide bound moderately and carbon dioxide poorly to CNTs [10]. The highly hydrophobic surface of CNTs enables the possibility of binding nonpolar polymers or cyclic hydrocarbons via van-der-Waals interactions. Thus, CNTs can be employed as hydrophobic interaction chromatography (HIC) resin which was demonstrated by Biesaga and Pyrzynska who were able to purify dicamba herbicides by the use of CNTs as chromatography resin [11]. For electrochemically modulated chromatography applications and the control of ion exchange by a potential switch, CNTs represent a very promising stationary phase material [12, 13]. Furthermore, an application as extraction material for nonpolar compounds has been demonstrated [14]. However, the agglomeration of the CNTs can reduce the efficiency of extraction processes. Superparamagnetic iron oxide nanoparticles (SPIONs) also possess interesting adsorbent properties, as several applications in wastewater treatment or medicine demonstrate [15–17]. In wastewater treatment, iron oxide nanoparticles are used for e.g. heavy metal removal, due to their low cost, their high specific surface area and their complexation properties [18]. In medicine, iron oxides can be used as contrast agents for magnetic resonance imaging, as drug delivery agent or for hyperthermia applications [17, 19]. Hence, it is quite interesting to mix these two materials to combine their beneficial properties; especially the conductivity for CNTs and the superparamagnetism for SPIONs are valuable for numerous application fields [20]. Decorating CNTs with SPIONs is a

possibility to enhance the dispersibility and the recyclability of CNTs due to the amphiphilic character of the hybrid surface. Thus, a composite unites the mixed-mode functionality of CNTs and iron oxides. Additionally, the decoration affects magnetic and electric properties of this material [15, 16, 21–25]. Furthermore, due to the superparamagnetism of the SPIONs, magnetic separation is possible with the hybrid composite [26]. Ajayan and Iijima started mixing SPIONs and CNTs by filling the tubes with nanoparticles [27]. Other possibilities include the binding of SPIONs to the CNT via polymer linkers or emulsifiers [18, 28, 29]. The decoration is also possible by solvothermal synthesis of iron oxide nanoparticles and direct attachment to multiwall CNTs [30, 31]. Nowadays, the prevalent method for decorating CNTs with SPIONs is the here also used acidic carboxylation of CNTs before the SPIONs are synthesized or applied to coat the CNTs [32, 33]. Typically, the iron oxide nanoparticles are seeded by the carboxylized CNTs and can be co-precipitated or synthesized by the Fenton's reaction directly on the surface [25, 34, 35]. While the carboxylation provides contact points for the SPIONs on the carbon surface, acidic treatment can lead to truncation of nanotubes [36]. Since the first combinations of SPIONs and CNTs multiple applications have been tested. The most challenging aspect in the synthesis is to control the aggregation of iron oxide nanoparticles in order to generate a homogeneous composite material [29, 36, 37]. Using carboxy groups as natural ligands for the iron oxide seeds for a co-precipitation process seems to be the best way to prevent strong aggregation effects and create a vastly decorated nanotube based material [25]. Therefore, we used established iron oxide synthesis routes for the attachment and decoration of carbon nanotubes [38, 39]. We investigated the surface modification of CNT with different acid treatments in order to

improve the binding of iron oxide nanoparticles to the CNTs. Magnetic nanoparticles are mixed with the modified CNTs and the resulting materials are thoroughly characterized. Previous studies demonstrated the suitability of such materials as extraction matrix for the separation of organic compounds [40]. We investigate the use of the resulting material as chromatography resin and study the binding behavior of amino acids as analytes. This work highlights the relationship of the wetting behavior of synthesized materials with the chromatography results where the materials are used as stationary phase. Furthermore, our study emphasizes the use of chromatography to describe the surface properties of materials and offers a direction to exploit chromatography as a methodology for material characterization and understanding of interaction behavior in the future.

Experimental

Materials

Carbon nanotubes (Baytubes C 150 P) were obtained from Bayer Materials Science AG, Germany. Ferric chloride ($FeCl_3 \cdot 6H_2O$) and sodium hydroxide (NaOH) were purchased from AppliChem GmbH, Germany. Ferrous chloride ($FeCl_2 \cdot 4H_2O$) was purchased from Bernd Kraft GmbH, Germany. Hydrochloric acid, nitric acid, hydrogen peroxide and sulfuric acid were obtained from Sigma-Aldrich. All materials were used as obtained.

Preparation of carboxylated CNTs (cCNTs)

CNTs (10 g) were suspended in a mixture of concentrated nitric (67%) and sulfuric acid (98%) (1:3 v/v) and stirred at room temperature for 18 h. The product was diluted with deionized water to a total volume of 2 L in order to stop the reaction. The carboxylated

CNTs were separated from the liquid with a paper filter and washed until a pH of 7 was reached. The resulting cCNTs were dried at 60 °C over night.

Co-precipitation of SPIONs on cCNTs

For the decoration of cCNT with MNP, a similar approach as described by Baykal et al. 2013 was chosen [25]. Dried cCNTs (2 g) were ultrasonicated in 800 mL deionized water in order to disagglomerate the tubes. The suspension was held at room temperature, stirred at 350 rpm and mixed with 14 g $FeCl_3$ 6 H_2O and 5.2 g $FeCl_2$ $4H_2O$. Sodium hydroxide (2 mol L^{-1}) was added to the suspension until a pH of 9.5 had been reached. The reaction was stopped after 30 minutes and the solid was filtered. The SPION decorated cCNTs are lyophilized in a freeze-drier Alpha 1-2 LDplus (Martin Christ Gefriertrocknungsmaschinen GmbH) prior to further analysis.

Transmission electron microscopy (TEM)

Low amounts of dried nanotubes were suspended in deionized water and disagglomerated with a Branson sonifier. The suspension was precipitated on a TEM grid and analyzed with a JEOL 100 CX. The micrographs were analyzed and a minimum of 100 particles were counted on each picture.

X-ray diffraction (XRD)

Dried samples were measured by a Stadi P diffractometer (STOE & Cie GmbH, Germany) equipped with a MoKα (λ = 0.7093 Å) source in transmission geometry. Data was collected in the range from 2° to 50° (2Θ). The software package STOE WinXPOW (STOE & Cie GmbH, Germany) was used for indexing and refinement purposes. The full

width at half maximum and the position of the <2 2 0> reflections were used to determine the primary particle diameter according to the Scherrer equation. A factor of 0.89, which is in agreement with spherical particles, was chosen.

X-ray photoelectron microscopy (XPS)

X-ray photoelectron spectroscopy was accomplished with a Leybold−Heraeus LHS 10 XPS system in ultrahigh vacuum (UHV) hosting a non-monochromatized Al Kα source (1486.7 eV). The powder samples were fixed on a vacuum compatible copper foil adhesive tape. The spectra were recorded at a constant pass energy mode set to 100 eV and a full width at half-maximum (FWHM) of ~1.1 eV. The C 1s (284.5 eV) peak corresponding to adventitious carbon was used as energy spectra of the C 1s; O 1s and Fe 2p regions were acquired by repeatedly scanning the same region 30 times in order to reduce statistical noise. All spectra were recorded in a UHV at a pressure below 5×10^{-8} mbar. The core level spectra were fitted by a mix of Gaussian and Lorentzian functions (Gaussian line width (0.7 eV) and Lorentzian line width (0.3 eV)).

Tensiometry

The contact angles of CNTs, cCNTs and cCNT-SPIONs were measured with a Krüss T100 MK3 tensiometer. Therefore, a packed bed of the nanotubes with a height of 2 cm was compressed uniformly for all samples. The capillarity of the packed beds was determined with the dissemination of n-hexane. Contact angles were determined with the liquids diiodo methane, dimethylsulfoxide, ethylene glycole, glycerine and deionized water. The free surface energy was calculated with the OWRK (Owens Wendt Rabel and Kälble) method [41].

151 Adsorption experiments

152 Adsorption isotherms of L-lysine at different concentrations in 100 mM phosphate buffer
153 at pH 7.8 were conducted with SPIONs, cCNTs and cCNT-SPIONs . The amino acid was
154 incubated for 24 h with the adsorbent and vigorously shaken at 25 °C. Different
155 concentrations of the amino acid were incubated with 1 g L^{-1} of cCNTs or cCNT-SPIONs
156 and with 2 g L^{-1} SPIONs. The supernatant concentration was determined by an assay
157 based on the Cayot method. This method is based on the photometric detection at 420
158 nm after modification of an amino acid with TNBSA at pH 8.5 [42].

159 Chromatography experiments

160 The dynamic binding capacities (DBC) of CNTs, cCNTs and cCNT-SPIONs were
161 determined with a chromatography column with a diameter of 6.6 mm. All samples were
162 packed dynamically under flowing water until a height of 6 to 8 cm is reached. The
163 chromatography experiments were conducted at a flow of 0.3 mL min^{-1}. The height
164 equivalent to a theoretical plate (HETP) and the dead time were determined with a 1 M
165 NaCl solution according to a modified van Deemter Equation: $HETP=L\frac{\sigma^2}{\mu^2}$; L is the column
166 length, σ represents the variance of the chromatography peak and μ is the first peak
167 moment. Furthermore, the asymmetry of the packed column was evaluated at 10 % peak
168 height prior to conducting the experiments: $A_s=\frac{b}{a}$; a represents the width of the front part
169 of the peak divided at peak maximum and b the width of the rear part. For calculating the
170 DBCs of different amino acids (glycine, L-lysine, L-histidine, L-glutamic acid and L-
171 cysteine), the solutions were adjusted to 10 mM at pH 6 with HCl or NaOH. The amino
172 acids were detected with a diode array detector at 200 nm. The columns were washed

with 30 mL water prior to loading with 15 mL of amino acid solution and washing with 20 mL of water followed by an elution with 20 mL of 1 M NaCl and another regeneration step of 20 mL water. The dynamic binding capacity was measured at 10% of the peak maximum. All experiments have been conducted in triplicates.

Results and Discussion

Multiwall carbon nanotubes are quite hydrophobic and therefore tend not to interact strongly with polar iron oxide nanoparticles. In order to make the CNTs more polar and allow for interactions with iron oxides, the surface was treated with nitric and sulfuric acid. This treatment generates surface defects and even charged surface groups, which act as seeds nanoparticle co-precipitation and as binding sites for iron oxide nanoparticles. Several methods and agents for the generation of defect sites were tested and analyzed with Raman spectroscopy (Fig. S1). Raman spectroscopy yields the ratios of the defect band (D) to the graphite band (G) [34, 35, 43, 44]. The ratio of the integral of G to D band is dependent on the laser wave length used [45]. However, the increase in this ratio is usually a good indicator for the oxidation of the nanotube surface and thus to identifying the best method for surface modification of CNTs [45–48]. While our results indicate a very high ratio for D:G after nitric acid treatment of the nanotubes suspension, the mix of nitric and sulfuric acid lead to a slight increase of this ratio (Table S1). For the further experiments only CNTs treated with the mix of nitric and sulfuric acid were used which represented the most reproducible method leading to nanotubes which can be packed in chromatography columns in accordance to our experiments and literature [48]. These nanotubes are referred to as carboxylated CNTs (cCNTs).

Iron oxide nanoparticles synthesized by co-precipitation in presence of cCNTs yield SPIONs with slightly larger average size as similarly synthesized particles without cCNTs (Fig. 1c). However, the size distribution is broader in the range of 5-20 nm and the particles synthesized with cCNTs are attached to the nanotubes. The synthesized composite material mainly possesses the properties of the iron oxide nanoparticles and is decorated homogeneously. The decoration of cCNTs with iron oxide nanoparticles which can be observed with transmission electron microscopy is in good agreement with literature [25, 29–31]. Our results indicate a homogeneous load of SPIONs on cCNTs as no larger aggregates of nanoparticles can be observed in the images (Fig. 1b).

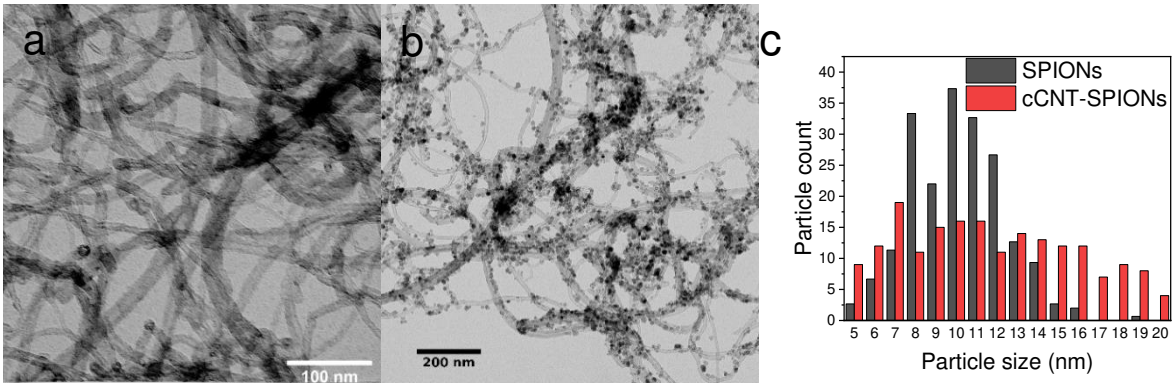

Fig. 1 TEM images of cCNTs **a** and cCNT-SPIONs **b**. Size distribution from four images and a count of minimum 30 particles per picture for each material **c**.

Magnetization measurements at room temperature indicate a superparamagnetic composite material with a saturation magnetization of 67 emu g^{-1} and no magnetic remanence (<1 emu g^{-1}). The saturation magnetization is only slightly lower than pure bare iron oxide nanoparticles and the shape of the hysteresis curve is similar (Fig. 2) [38, 49, 50]. Hence, surface layer and core composition of SPIONs and cCNT-SPIONs composites are similar [50]. The crystallographic analysis of the composite material

shows a spinel structure corresponding to either magnetite or maghemite, while no crystalline structure of CNTs can be observed (Fig. 2b) [30, 50]. The signal at 11.8° occurring in CNTs and cCNTs can be indexed as the <0 0 2> reflection of the hexagonal graphite structure [16]. The decoration of cCNTs with iron oxide nanoparticles leads to the occurrence of the reflections: <1 1 1> at 5.4° <2 2 0> at 13.7°, <3 1 1> at 16.1°, <4 0 0> at 19.4°, <4 2 2> at 23.8°, <5 1 1> at 25.3° and <4 4 0> at 25.6° [22, 34]. These reflections are consistent with the standard XRD data for the cubic phase Fe_3O_4 (JCPDS no. 89-4319) with a face-centered cubic structure and our own reference SPIONs [16, 25]. The reflections of the composite material show a larger FWHM resulting in a smaller Scherrer diameter of the crystalline material. This behavior can be explained with the larger particle size distribution of the composite material as observed with TEM, and the additional nucleation seeds on the surface of cCNTs [39]. Higher numbers of nucleation seeds usually lead to smaller primary crystallites [29, 39]. The magnetization as well as the diffraction patterns are in good agreement with other decoration methods such as electrostatic modification through polyethyleneimine or polyacrylate acid [15, 20]. The intensity of the reflection corresponding to graphite is similar in the pure material and the composite material and no significant changes can be observed. However, the intensity of the reflections corresponding to iron oxide structures demonstrate a much more intense signal.

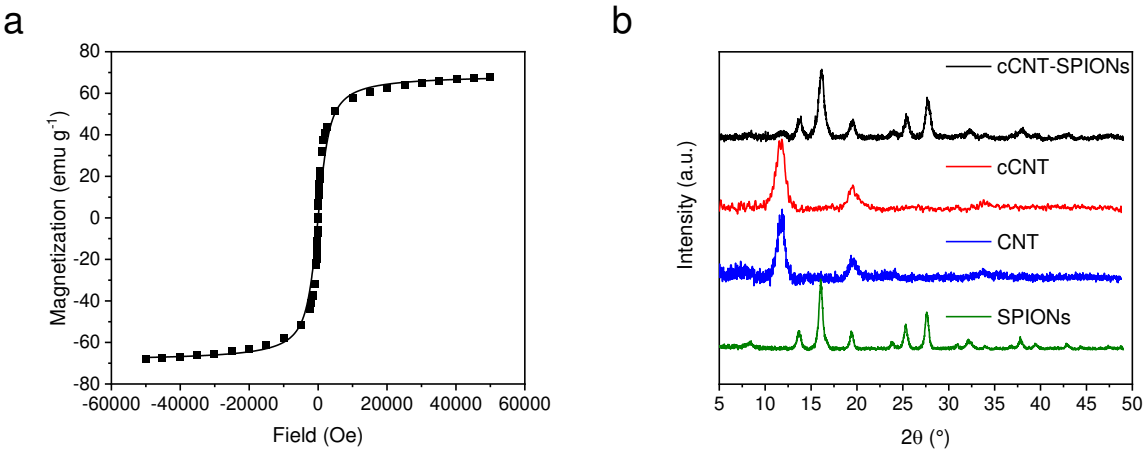

Fig. 2 Powder XRD patterns of cCNT-SPIONs, cCNTs, CNTs and SPIONs obtained with a MoKα source **a** and magnetic hysteresis curve obtained with a SQUID from -50000 to 50000 Oe at 300 K **b**.

Hence, the composite material combines the properties of carbon nanotubes and magnetic nanoparticles. X-ray photoelectron spectroscopy, which is a very surface sensitive method shows the attachment of iron oxide to cCNTs (Fig. S2). Here, magnetite and/or maghemite are present since the F $2p^{3/2}$ band of the cCNT-SPIONs shows a maximum at 711 eV and the Fe $2p^{1/2}$ shows a maximum at 724 eV [30, 50]. The shape of the shake up satellites also indicates the presence of magnetite rather than hematite [50, 51]. The O 1s region indicates C-O, and COO^- bonds for both cCNTs and cCNT-SPIONs, while the composite material demonstrates another band at 529.5 eV which corresponds to the presence of Fe-O bonds [30, 34]. The bonds between carbon and oxygen in the O 1s region are in good agreement with the observations of the C 1s region, which also indicates differently oxidized carbon species (Fig. 3). Here, not only carboxy groups (289 eV) but other C-O bonds (286-287.5 eV) as well as sp^2 hybridized carbon

(284.5 eV) corresponding to carbon from the backbone structure of CNTs can be observed [34, 44].

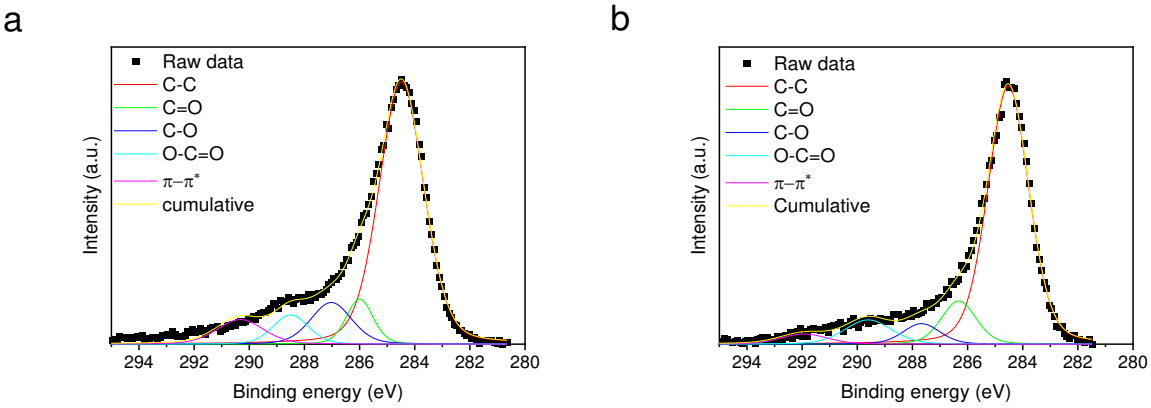

Fig. 3 XP spectra in the range of C 1s of cCNTs **a** and cCNT-SPIONs **b**. The spectra are fitted with a combination of Gaussian and Lorentzian functions with the program Origin.

The decoration of cCNTs with SPIONS can be observed with ATR-IR spectroscopy as well. In Fig. 4, the band at 550 cm^{-1} corresponding to a T_{1u} vibration of magnetite crystals is most prominent for the composite material [16, 51]. On the carboxylized CNTs the COO^- symmetric and asymmetric stretch vibrations corresponding to the carboxy group can be observed at 1325, 1400 (s) and 1624 cm^{-1} (as), respectively [16, 29, 43, 52]. Furthermore, the O-H stretch vibrations around 3250 cm^{-1} indicate the presence of carboxy groups on the cCNTs [16, 22, 25, 43]. The decrease of intensity for the peaks corresponding to C-O vibrations is a good indicator for a homogeneous coating.

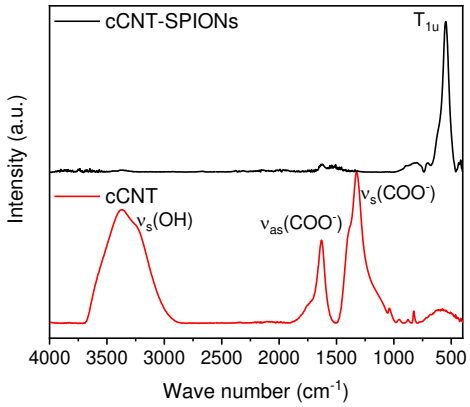

Fig. 4 ATR-IR spectra of cCNT-SPIONs and cCNTs.

The zeta potential of the composite material is only slightly higher than the zeta potential of bare SPIONs, even though the acidic treatment should result in a highly negatively charged material. We were not able to conduct zeta potential measurements of CNTs which tend to aggregate in aqueous environments. The isoelectric point of the composite material is still in the neutral range with pH 7.5 compared to pH 6.5 for the bare nanoparticles (Fig. 5a) [50]. This behavior suggests a good coating or decoration of the cCNTs with iron oxide nanoparticles and supports the other analytical characterizations of the composite. Furthermore, the behavior of the zeta potential is amphiphilic and similar for both materials with increasing and decreasing pH, which also indicates iron oxides being the most prominent surface species. We observe a very similar behavior for wetting experiments with the capillary rise method (Fig. S3). Here, the surface free energy as well as the polar and dispersive share, yielded by multiple experiments with different solvents, are similar for composite and bare iron oxide nanoparticles. The capillarity of the materials is determined with ethylene glycole for bare carbon nanotubes as described in literature [53, 54]. For all other materials, hexane as fluid with a very low surface tension (18.4 mJ

278 m^{-2}) was chosen to determine the capillarity. Bare iron oxide nanoparticles possess a total
279 surface free energy of 55.9 mJ m^{-2}, while the composite material has a surface energy of
280 47.1 mJ m^{-2} (Fig. 5b). The composite material has a slightly higher polar share, However,
281 the untreated CNTs and the cCNT behave completely different. The untreated CNTs
282 show a high dispersive surface free energy, while the cCNTs are highly polar according
283 to the method from Owens Wendt Rabel and Kälble [41]. From this method the polar and
284 dispersive shares of the wetting liquids and the resulting contact angle derived from
285 capillary rise experiments can be compared (Fig. S4). The surface free energy of the
286 CNTs obtained from this method is slightly higher than the results obtained from Dresel
287 and Teipel who also performed capillary rise experiments with Baytube CNTs [53]. The
288 tensiometry results obtained with the capillary rise method are an interesting indicator in
289 order to describe the differences such as polarity and wetting with water of nanomaterial
290 surfaces. However, especially with nanostructured surfaces and nanostructured
291 capillaries, this method can be prone to errors. Here, all materials show a high specific
292 surface area (Figure S5). Bare iron oxide nanoparticles demonstrate a specific surface
293 area of 110 m^2 g^{-1}, the cCNTs possess a specific surface area of 228 m^2 g^{-1} and the
294 composite material shows a specific surface area of 131 m^2 g^{-1}. This specific surface area
295 is in a similar range, especially when considering the volumetric surface area since the
296 densities of cCNTs (1.46 g cm^{-1}), cCNT-SPIONs (2.38 g cm^{-1}) and SPIONs (3.8 g cm^{-1})
297 vary significantly. The density of CNTs is in good agreement within the variation of density
298 for carbon nanotubes [47].

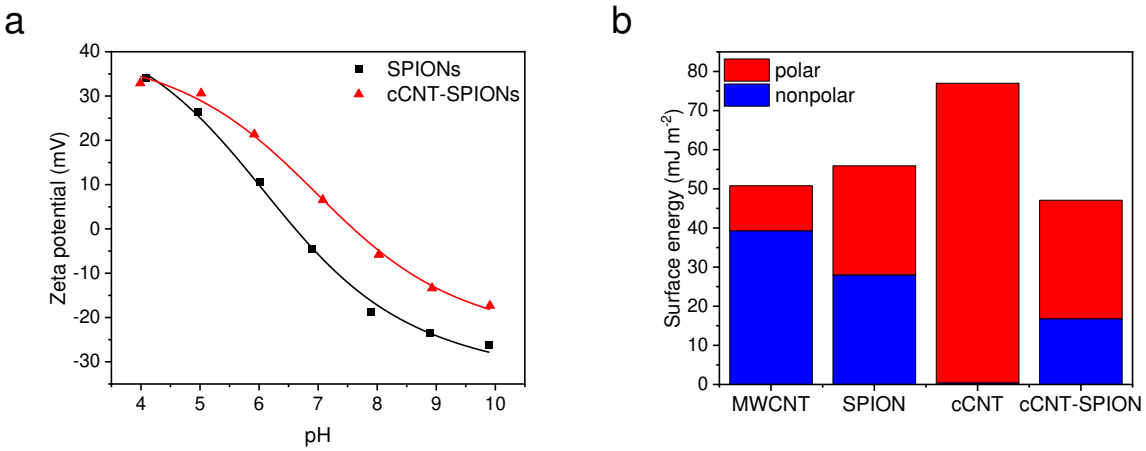

Fig. 5 Zeta potential of SPIONs and cCNT-SPIONs from pH 4 to 10 **a** and surface free energy obtained from capillary rise experiments with the OWRK method **b**

In order to make use of the composite material for solid phase extraction and chromatography processes, the static and dynamic binding capacity of amino acids has been compared. One of the main goals of this study was to verify if the composite material can be used in a chromatography system, where iron oxide nanoparticles can act as stationary phase. The bare nanoparticles cannot be used as a stationary phase in a chromatography column on their own due to the large pressure drop and possible losses through the filter. Thus, the binding behavior of amino acids to bare nanoparticles can only be compared with adsorption isotherms in equilibrium. In Fig. 6a, a similar behavior of the adsorption isotherm of L-lysine on cCNT-SPIONs, and SPIONs can be observed. The equilibrium binding constant (K_D) is in a similar range (0.17 g L^{-1} for cCNT-SPIONs and 0.72 g L^{-1} for SPIONs) and the large difference in the maximum binding capacity (0.91 g g^{-1} for cCNT-SPIONs and 0.15 g g^{-1} for SPIONs). The differences of affinity and binding capacity can be explained by strong electrostatic interactions between lysine and negatively charged materials such as cCNTs compared to the interactions with

amphiphilic iron oxides [55]. L-lysine was chosen since this amino acid is much easier to detect with the TNBSA method compared to other amino acids [42]. The maximum load is in a similar range as literature for cationic adsorptives such as methylene blue or aniline on iron oxide decorated carbon nanotubes [16, 44]. For the dynamic binding capacity, which was obtained from inverse liquid chromatography experiments, huge differences between cCNTs and cCNT-SPIONs can be observed. While amino acids such as the positively charged L-lysine shows a higher DBC on cCNTs, the negatively charged L-glutamate shows a significantly higher DBC on cCNT-SPIONs. This behavior is in good agreement with literature, where L-glutamate demonstrates a high affinity to iron oxide nanoparticles [52, 56]. The high affinity of the L-lysine to cCNTs can be explained by electrostatic interactions between the positively charged amino acid and the negatively charged carboxy functionalized nanotubes. Glycine shows a higher dynamic binding capacity to cCNT-SPIONs than to cCNTs, which might be explained by the more amphiphilic character of iron oxide surfaces. The high dynamic binding capacity of L-cysteine to the composite material is in good agreement with the literature and the formation of cystine due to interaction of L-cysteine with iron ions [52]. L-histidine shows a high dynamic binding capacity to all materials since electrostatic, coordinative and hydrophobic interactions are possible. While the column packed with cCNT-SPIONs shows a higher HETP value compared to CNTs and cCNTs, the asymmetry of cCNT-SPIONs is similar to cCNTs and with around 0.7 in a range which allows the analysis of breakthrough curves (Fig. S6 and Table S2). The porosity of all systems is in a similar range between 0.78 and 0.94 and in good agreement with other stationary phases used for inverse chromatography experiments [57].

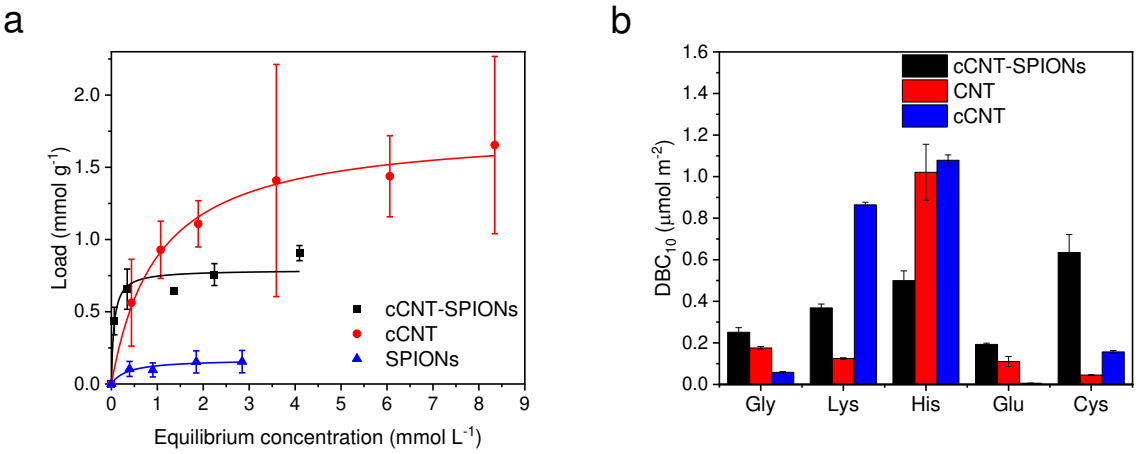

339

340 **Fig. 6** Static binding capacities of L-lysine with cCNTs, cCNT-SPIONs and SPIONs at pH
341 7.8 with 100 mM phosphate buffer **a**. Dynamic binding capacities at 10% of the
342 breakthrough of cCNT-SPIONs, CNTs and cCNTs obtained from inverse chromatography
343 experiments with different amino acids at pH 6 **b**.

344 **Conclusion**

345 In this study, a composite material combining superparamagnetic iron oxide nanoparticles
346 and carbon nanotubes has been synthesized. The first aim of this study was to investigate
347 the surface properties of the composite material with the goal of understanding the share
348 of each initial material to the final composite. Furthermore, the study is a proof of concept
349 to test the effect of such materials for molecule separation with focus on the retention
350 behavior of amino acids with liquid chromatography. The idea was to combine the surface
351 reactivity of iron oxide nanoparticles with the packing properties of carbon nanotubes, a
352 chromatographic matrix which leads to very low pressure drop. It was possible to
353 establish a chromatography system and characterize the interaction of positively or
354 negatively charged, and uncharged amino acids with the composite material. Hence, this

355 material might be a good indicator for interactions with a hybrid matrix. However, not only
356 the use in a chromatography system but also processes such as solid phase extraction
357 are possible with the created material due to the high saturation magnetization obtained
358 with the described decoration procedure [26]. The magnetic properties allow for a simple
359 magnetic separation, while the carbon nanotubes regulate the macroscopic structure and
360 the accessibility of target molecules to the surface. With this study we want to emphasize
361 the similarity of magnetic separation and analytical chromatography since similar
362 materials and adsorption equilibria can be demonstrated, even though there are multiple
363 differences. For the future exploitation of this unique magnetic material, particularly its
364 hydrodynamic properties seem interesting and should be analyzed, e.g. for mixed-mode
365 applications as in chromatography. Furthermore, the electrical properties of the
366 composite might pave the way for further electrochemical applications. Tabassum et al.
367 reviewed multiple applications for metal-based nanoparticles confined into carbon
368 nanotubes, which open up opportunities for electro-catalysis, energy conversion and
369 storage devices [58].
370 The understanding and design of composite materials and the description of surface and
371 interface properties is challenging. Nevertheless, hybrid and composite materials have
372 the power to open doors for higher complexity in applications in all fields in the future.
373 Chromatography is somehow a pioneering technology, which shows applicability for all
374 possible kinds of target compounds and offers a very broad portfolio of methods and of
375 processing solutions. We think that materials as the one we present in this study are
376 necessary to understand the share of different properties in a particular processing form

and how materials of different composition impact the final output of processes based on interactions at the solid-liquid interface.

Declarations

Availability of data and materials

All data generated or analyzed during this study are included in this published article and its supplementary information files.

Competing interests

The authors declare that they have no competing interests

Funding

This study was financially supported by the Federal Ministry of Education and Research (Grant number 031A173A and 13XP5038A) and by the German Federation of Industrial Research Associations (IGF/AiF–Arbeitsgemeinschaft industrieller Forschungsvereinigungen, FKZ 17472 N/2)

Authors' contributions

SS and MB designed the study and all experiments. FZ and ND synthesized the materials and performed the experiments. SS, PF-G and SB wrote the manuscript. All authors discussed the results and commented on the manuscript. All authors read and approved the final manuscript.

Acknowledgements

We would like to thank Dr. Marianne Hanzlik for help with TEM, Prof. Tom Nilges for the provision of XRD, Prof. Thomas Fässler for the provision of SQUID and Prof. Sebastian Günther for help with the XPS.

400

401 References

402 1. Iijima S (1991) Helical microtubules of graphitic carbon. Nature 354: 56–58.
403 https://doi.org/10.1038/354056a0

404 2. Baughman RH, Zakhidov AA, Heer WA de (2002) Carbon nanotubes--the route toward
405 applications. Science 297: 787–792. https://doi.org/10.1126/science.1060928

406 3. Venkataraman A, Amadi EV, Chen Y et al. (2019) Carbon Nanotube Assembly and
407 Integration for Applications. Nanoscale Res Lett 14: 220. https://doi.org/10.1186/s11671-
408 019-3046-3

409 4. Eatemadi A, Daraee H, Karimkhanloo H et al. (2014) Carbon nanotubes: properties,
410 synthesis, purification, and medical applications. Nanoscale Res Lett 9: 393.
411 https://doi.org/10.1186/1556-276X-9-393

412 5. Elhissi AMA, Ahmed W, Hassan IU et al. (2012) Carbon nanotubes in cancer therapy and
413 drug delivery. J. Drug Delivery 2012: 837327. https://doi.org/10.1155/2012/837327

414 6. Gupta VK, Agarwal S, Saleh TA (2011) Chromium removal by combining the magnetic
415 properties of iron oxide with adsorption properties of carbon nanotubes. Water Res.
416 45: 2207–2212. https://doi.org/10.1016/j.watres.2011.01.012

417 7. Huang H, Yuan Q, Shah JS et al. (2011) A new family of folate-decorated and carbon
418 nanotube-mediated drug delivery system: synthesis and drug delivery response. Adv. Drug
419 Delivery Rev. 63: 1332–1339. https://doi.org/10.1016/j.addr.2011.04.001

8. Kim J-W, Moon H-M, Tung S et al. (2009 - 2009) Highly effective bacterial removal system using carbon nanotube clusters. In: 2009 4th IEEE International Conference on Nano/Micro Engineered and Molecular Systems. IEEE, pp 1062–1064

9. Trojanowicz M (2006) Analytical applications of carbon nanotubes: a review. TrAC Trends in Analytical Chemistry 25: 480–489. https://doi.org/10.1016/j.trac.2005.11.008

10. Long RQ, Yang RT (2001) Carbon Nanotubes as a Superior Sorbent for Nitrogen Oxides. Ind Eng Chem Res 40: 4288–4291. https://doi.org/10.1021/ie000976k

11. Biesaga M, Pyrzynska K (2006) The evaluation of carbon nanotubes as a sorbent for dicamba herbicide. J. Sep. Sci. 29: 2241–2244. https://doi.org/10.1002/jssc.200600109

12. Brammen M, Fraga-García P, Berensmeier S (2017) Carbon nanotubes-A resin for electrochemically modulated liquid chromatography. J. Sep. Sci. 40: 1176–1183. https://doi.org/10.1002/jssc.201601102

13. Trunzer T, Stummvoll T, Porzenheim M et al. (2020) A Carbon Nanotube Packed Bed Electrode for Small Molecule Electrosorption: An Electrochemical and Chromatographic Approach for Process Description. Applied Sciences 10: 1133. https://doi.org/10.3390/app10031133

14. Carrillo-Carrión C, Lucena R, Cárdenas S et al. (2007) Surfactant-coated carbon nanotubes as pseudophases in liquid-liquid extraction. Analyst 132: 551–559. https://doi.org/10.1039/B701019B

15. Yang D, Yang F, Hu J et al. (2009) Hydrophilic multi-walled carbon nanotubes decorated with magnetite nanoparticles as lymphatic targeted drug delivery vehicles. Chem. Comm.: 4447–4449. https://doi.org/10.1039/B908012K

16. Ai L, Zhang C, Liao F et al. (2011) Removal of methylene blue from aqueous solution with magnetite loaded multi-wall carbon nanotube: kinetic, isotherm and mechanism analysis. J Hazard Mater 198: 282–290. https://doi.org/10.1016/j.jhazmat.2011.10.041

17. Bae H, Ahmad T, Rhee I et al. (2012) Carbon-coated iron oxide nanoparticles as contrast agents in magnetic resonance imaging. Nanoscale Res Lett 7: 44. https://doi.org/10.1186/1556-276X-7-44

18. Maggini L, Raquez J-M, Marega R et al. (2013) Magnetic poly(vinylpyridine)-coated carbon nanotubes: an efficient supramolecular tool for wastewater purification. ChemSusChem 6: 367–373. https://doi.org/10.1002/cssc.201200413

19. Cabana L, Bourgognon M, Wang JT-W et al. (2016) The Shortening of MWNT-SPION Hybrids by Steam Treatment Improves Their Magnetic Resonance Imaging Properties In Vitro and In Vivo. Small 12: 2893–2905. https://doi.org/10.1002/smll.201502721

20. Zhang Q, Zhu M, Zhang Q et al. (2009) The formation of magnetite nanoparticles on the sidewalls of multi-walled carbon nanotubes. Composites Science and Technology 69: 633–638. https://doi.org/10.1016/j.compscitech.2008.12.011

21. Yu W-J, Hou P-X, Li F et al. (2012) Improved electrochemical performance of Fe2O3 nanoparticles confined in carbon nanotubes. J Mater Chem 22: 13756. https://doi.org/10.1039/c2jm31442h

22. Rahman MM, Hussain MM, Asiri AM (2017) Fabrication of 3-methoxyphenol sensor based on Fe3O4 decorated carbon nanotube nanocomposites for environmental safety: Real sample analyses. PLoS ONE 12: e0177817. https://doi.org/10.1371/journal.pone.0177817

23. Liu S, Sun S, You X-Z (2014) Inorganic nanostructured materials for high performance electrochemical supercapacitors. Nanoscale 6: 2037–2045. https://doi.org/10.1039/c3nr05403a

24. Stoffelbach F, Aqil A, Jérôme C et al. (2005) An easy and economically viable route for the decoration of carbon nanotubes by magnetite nanoparticles, and their orientation in a magnetic field. Chem Commun (Camb): 4532–4533. https://doi.org/10.1039/b506758h

25. Baykal A, Senel M, Unal B et al. (2013) Acid Functionalized Multiwall Carbon Nanotube/Magnetite (MWCNT)-COOH/Fe3O4 Hybrid: Synthesis, Characterization and Conductivity Evaluation. J. Inorg. Organomet. Polym. (Journal of Inorganic and Organometallic Polymers and Materials) 23: 726–735. https://doi.org/10.1007/s10904-013-9839-4

26. Xu J, Zheng J, Tian J et al. (2013) New materials in solid-phase microextraction. TrAC Trends in Analytical Chemistry 47: 68–83. https://doi.org/10.1016/j.trac.2013.02.012

27. Ajayan PM, lijima S (1993) Capillarity-induced filling of carbon nanotubes. Nature 361: 333–334. https://doi.org/10.1038/361333a0

28. Mo Z, He J, Wang J et al. (2013) Preparation and characterisation of PPy/NanoGs/Fe 3 O 4 conductive and magnetic nanocomposites. J. Exp. Nanosci. 8: 113–120. https://doi.org/10.1080/17458080.2012.674218

29. Shi D, Cheng JP, Liu F et al. (2010) Controlling the size and size distribution of magnetite nanoparticles on carbon nanotubes. Journal of Alloys and Compounds 502: 365–370. https://doi.org/10.1016/j.jallcom.2010.04.169

30. Wang H, Cao L, Yan S et al. (2009) An efficient method for decoration of the multiwalled carbon nanotubes with nearly monodispersed magnetite nanoparticles. Materials Science and Engineering: B 164: 191–194. https://doi.org/10.1016/j.mseb.2009.08.012

31. Wang Z, Wu L, Zhou J et al. (2013) Magnetite Nanocrystals on Multiwalled Carbon Nanotubes as a Synergistic Microwave Absorber. J Phys Chem C 117: 5446–5452. https://doi.org/10.1021/jp4000544

32. Dai L, He P, Li S (2003) Functionalized surfaces based on polymers and carbon nanotubes for some biomedical and optoelectronic applications. Nanotechnology 14: 1081–1097. https://doi.org/10.1088/0957-4484/14/10/305

33. Georgakilas V, Tzitzios V, Gournis D et al. (2005) Attachment of Magnetic Nanoparticles on Carbon Nanotubes and Their Soluble Derivatives. Chem Mater 17: 1613–1617. https://doi.org/10.1021/cm0483590

34. Yu F, Chen J, Chen L et al. (2012) Magnetic carbon nanotubes synthesis by Fenton's reagent method and their potential application for removal of azo dye from aqueous solution. J. Colloid Interface Sci. 378: 175–183. https://doi.org/10.1016/j.jcis.2012.04.024.

35. Zhong W, Liu P, Tang Z et al. (2012) Facile Approach for Superparamagnetic CNT-Fe 3 O 4 /Polystyrene Tricomponent Nanocomposite via Synergetic Dispersion. Ind Eng Chem Res 51: 12017–12024. https://doi.org/10.1021/ie300891h

36. Jia B, Gao L (2007) Fabrication of "tadpole"-like magnetite/multiwalled carbon nanotube heterojunctions and their self-assembly under external magnetic field. J. Phys. Chem. B 111: 5337–5343. https://doi.org/10.1021/jp070675p

37. Jia B, Gao L, Sun J (2007) Self-assembly of magnetite beads along multiwalled carbon nanotubes via a simple hydrothermal process. Carbon 45: 1476–1481. https://doi.org/10.1016/j.carbon.2007.03.025

38. Roth H-C, Schwaminger SP, Schindler M et al. (2015) Influencing factors in the CO-precipitation process of superparamagnetic iron oxide nano particles: A model based study. Journal of Magnetism and Magnetic Materials 377: 81–89. https://doi.org/10.1016/j.jmmm.2014.10.074

39. Schwaminger SP, Syhr C, Berensmeier S (2020) Controlled Synthesis of Magnetic Iron Oxide Nanoparticles: Magnetite or Maghemite? Crystals 10: 214. https://doi.org/10.3390/cryst10030214

40. Moazzen M, Mousavi Khaneghah A, Shariatifar N et al. (2019) Multi-walled carbon nanotubes modified with iron oxide and silver nanoparticles (MWCNT-Fe3O4/Ag) as a novel adsorbent for determining PAEs in carbonated soft drinks using magnetic SPE-GC/MS method. Arabian Journal of Chemistry 12: 476–488. https://doi.org/10.1016/j.arabjc.2018.03.003

41. Owens DK, Wendt RC (1969) Estimation of the surface free energy of polymers. J Appl Polym Sci 13: 1741–1747. https://doi.org/10.1002/app.1969.070130815

42. Cayot P, Tainturier G (1997) The quantification of protein amino groups by the trinitrobenzenesulfonic acid method: a reexamination. Anal Biochem 249: 184–200. https://doi.org/10.1006/abio.1997.2161

43. Cheng JP, Yu J, Shi D et al. (2012) Controllable one-step synthesis of magnetite/carbon nanotubes composite and its electrochemical properties. Appl Phys A 106: 837–842. https://doi.org/10.1007/s00339-012-6786-9

44. Shao D, Hu J, Chen C et al. (2010) Polyaniline Multiwalled Carbon Nanotube Magnetic Composite Prepared by Plasma-Induced Graft Technique and Its Application for Removal of Aniline and Phenol. J Phys Chem C 114: 21524–21530. https://doi.org/10.1021/jp107492g

45. Gouadec G, Colomban P (2007) Raman Spectroscopy of nanomaterials: How spectra relate to disorder, particle size and mechanical properties. Progress in Crystal Growth and Characterization of Materials 53: 1–56. https://doi.org/10.1016/j.pcrysgrow.2007.01.001

46. Anik U, Cevik S, Pumera M (2010) Effect of Nitric Acid "Washing" Procedure on Electrochemical Behavior of Carbon Nanotubes and Glassy Carbon μ-Particles. Nanoscale Res Lett 5: 846–852. https://doi.org/10.1007/s11671-010-9573-6

47. Lehman JH, Terrones M, Mansfield E et al. (2011) Evaluating the characteristics of multiwall carbon nanotubes. Carbon 49: 2581–2602. https://doi.org/10.1016/j.carbon.2011.03.028

48. Osswald S, Havel M, Gogotsi Y (2007) Monitoring oxidation of multiwalled carbon nanotubes by Raman spectroscopy. J Raman Spectrosc 38: 728–736. https://doi.org/10.1002/jrs.1686

49. Thomas JA, Schnell F, Kaveh-Baghbaderani Y et al. (2020) Immunomagnetic Separation of Microorganisms with Iron Oxide Nanoparticles. Chemosensors 8: 17. https://doi.org/10.3390/chemosensors8010017

50. Schwaminger SP, Bauer D, Fraga-García P et al. (2017) Oxidation of magnetite nanoparticles: impact on surface and crystal properties. CrystEngComm 19: 246–255. https://doi.org/10.1039/C6CE02421A

51. Schwaminger SP, Fraga-García P, Selbach F et al. (2017) Bio-nano interactions: cellulase on iron oxide nanoparticle surfaces. Adsorption 23: 281–292. https://doi.org/10.1007/s10450-016-9849-y

52. Schwaminger SP, Fraga García P, Merck GK et al. (2015) Nature of Interactions of Amino Acids with Bare Magnetite Nanoparticles. J Phys Chem C 119: 23032–23041. https://doi.org/10.1021/acs.jpcc.5b07195

53. Dresel A, Teipel U (2014) Benetzungsverhalten von Kohlenstoffnanoröhren. Chemie Ingenieur Technik 86: 253–261. https://doi.org/10.1002/cite.201300165

54. Schwaminger SP, Begovic B, Schick L et al. (2018) Potential-Controlled Tensiometry: A Tool for Understanding Wetting and Surface Properties of Conductive Powders by Electroimbibition. Anal Chem 90: 14131–14136. https://doi.org/10.1021/acs.analchem.8b03475

562 55. Bag S, Rauwolf S, Suyetin M et al. (2020) Buffer Influence on the Amino Acid Silica
563 Interaction. Chemphyschem. https://doi.org/10.1002/cphc.202000572

564 56. Schwaminger SP, Blank-Shim SA, Scheifele I et al. (2017) Peptide binding to metal oxide
565 nanoparticles. Faraday Discuss 204: 233–250. https://doi.org/10.1039/C7FD00105C

566 57. Bednar I, Tscheliessnig R, Berger E et al. (2012) Surface energies of hydrophobic
567 interaction chromatography media by inverse liquid chromatography. J Chromatogr A
568 1220: 115–121. https://doi.org/10.1016/j.chroma.2011.11.001

569 58. Tabassum H, Mahmood A, Zhu B et al. (2019) Recent advances in confining metal-based
570 nanoparticles into carbon nanotubes for electrochemical energy conversion and storage
571 devices. Energy Environ. Sci. 12: 2924–2956. https://doi.org/10.1039/c9ee00315k

572

Figures

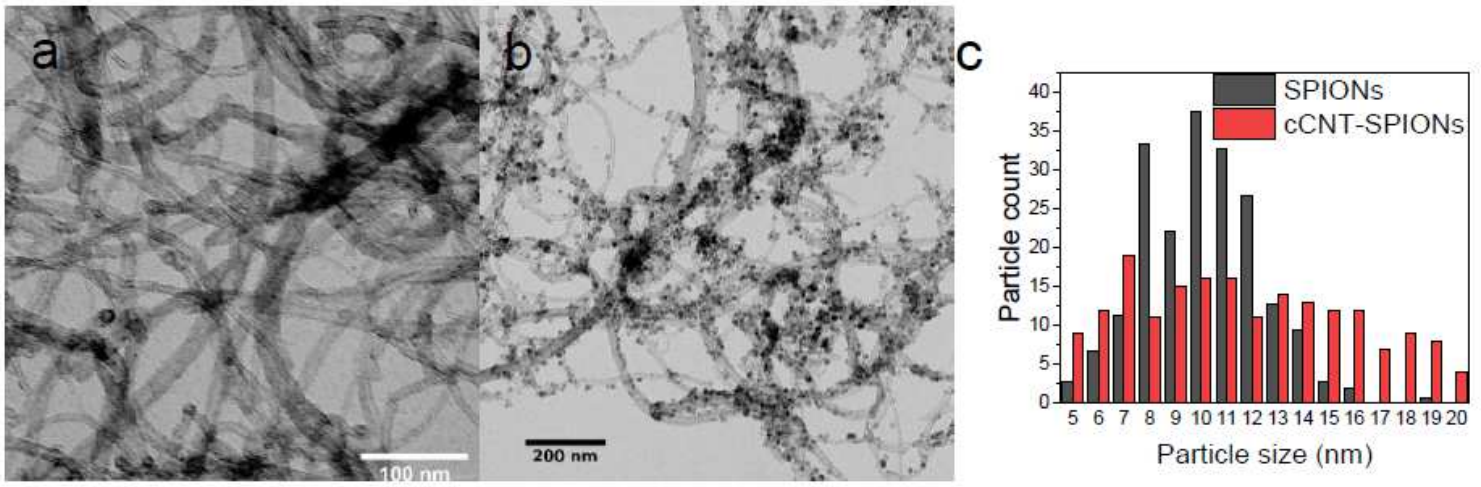

Figure 1

TEM images of cCNTs a and cCNT-SPIONs b. Size distribution from four images and a count of minimum 30 particles per picture for each material c.

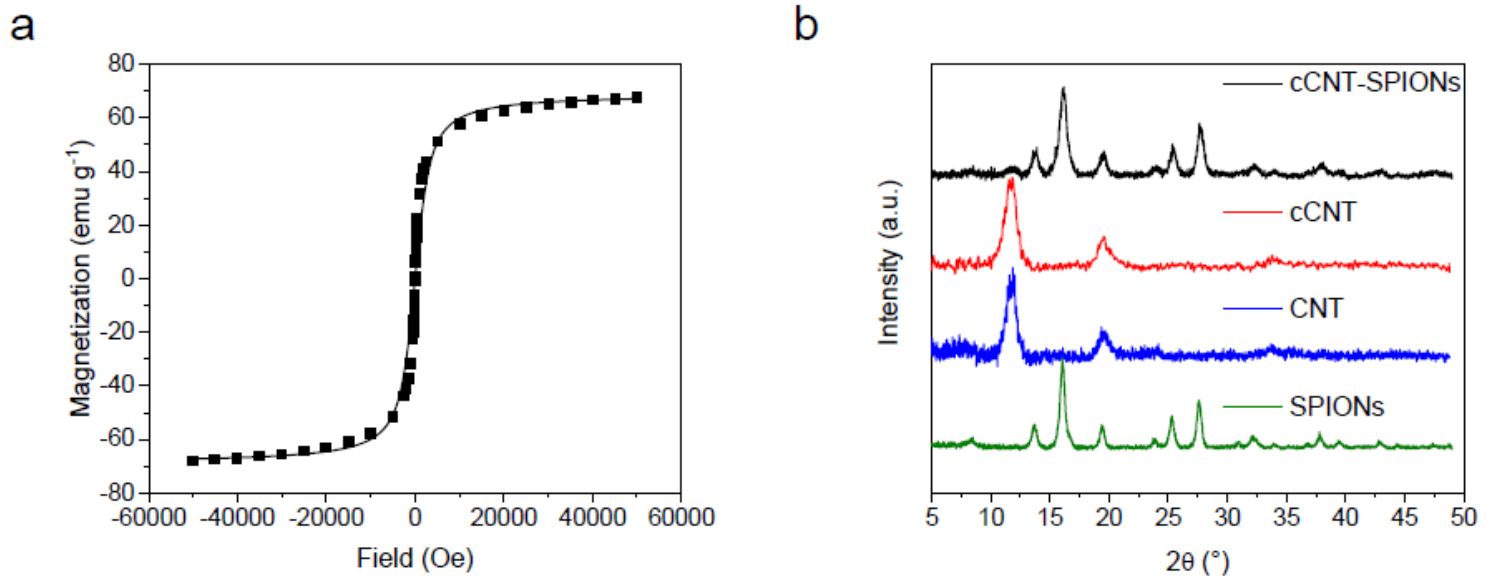

Figure 2

Powder XRD patterns of cCNT-SPIONs, cCNTs, CNTs and SPIONs obtained with a MoKα source a and magnetic hysteresis curve obtained with a SQUID from -50000 to 50000 Oe at 300 K b.

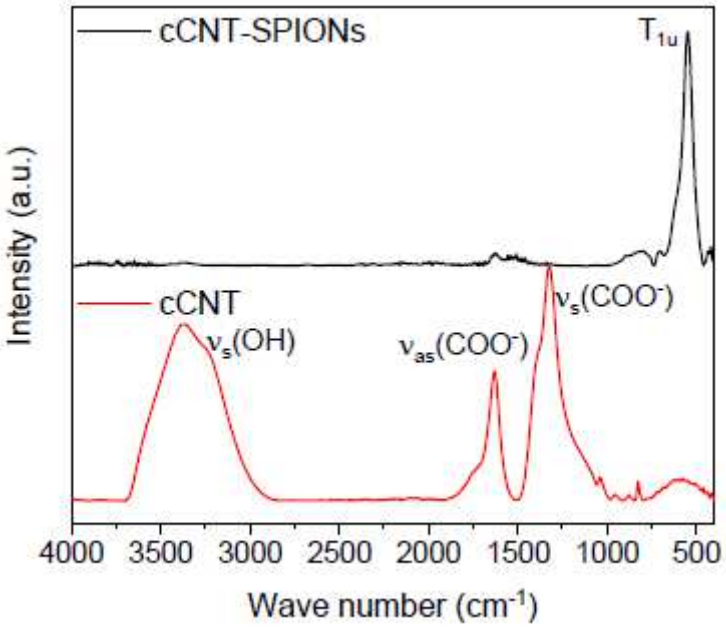

Figure 3

XP spectra in the range of C 1s of cCNTs a and cCNT-SPIONs b. The spectra are fitted with a combination of Gaussian and Lorentzian functions with the program Origin.

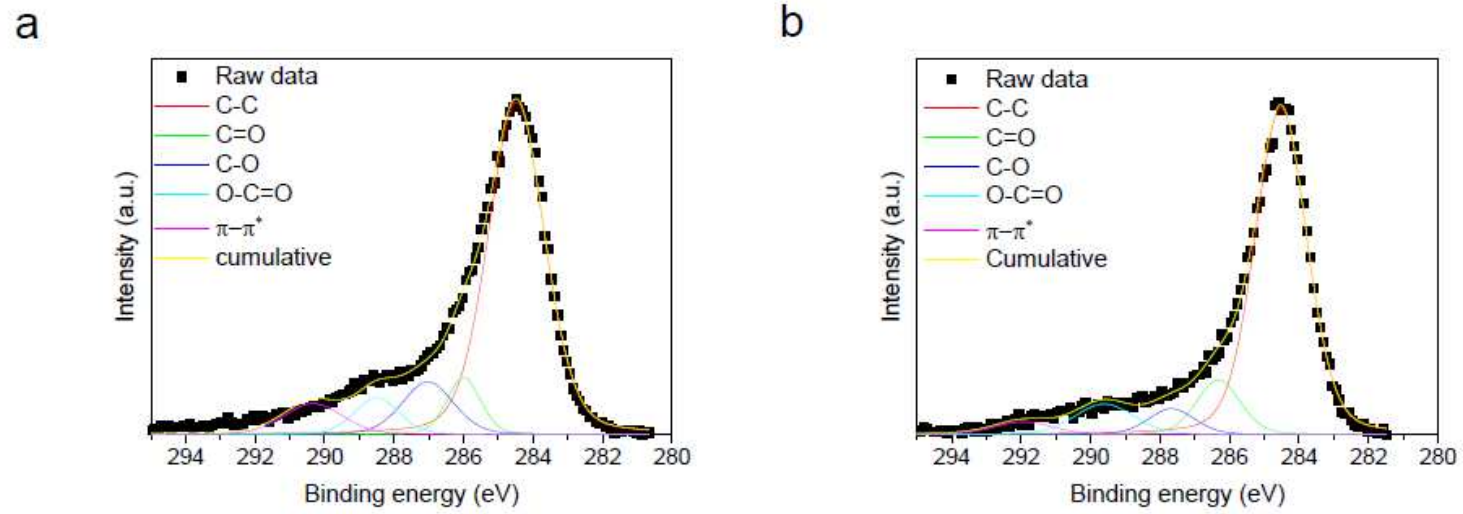

Figure 4

ATR-IR spectra of cCNT-SPIONs and cCNTs.

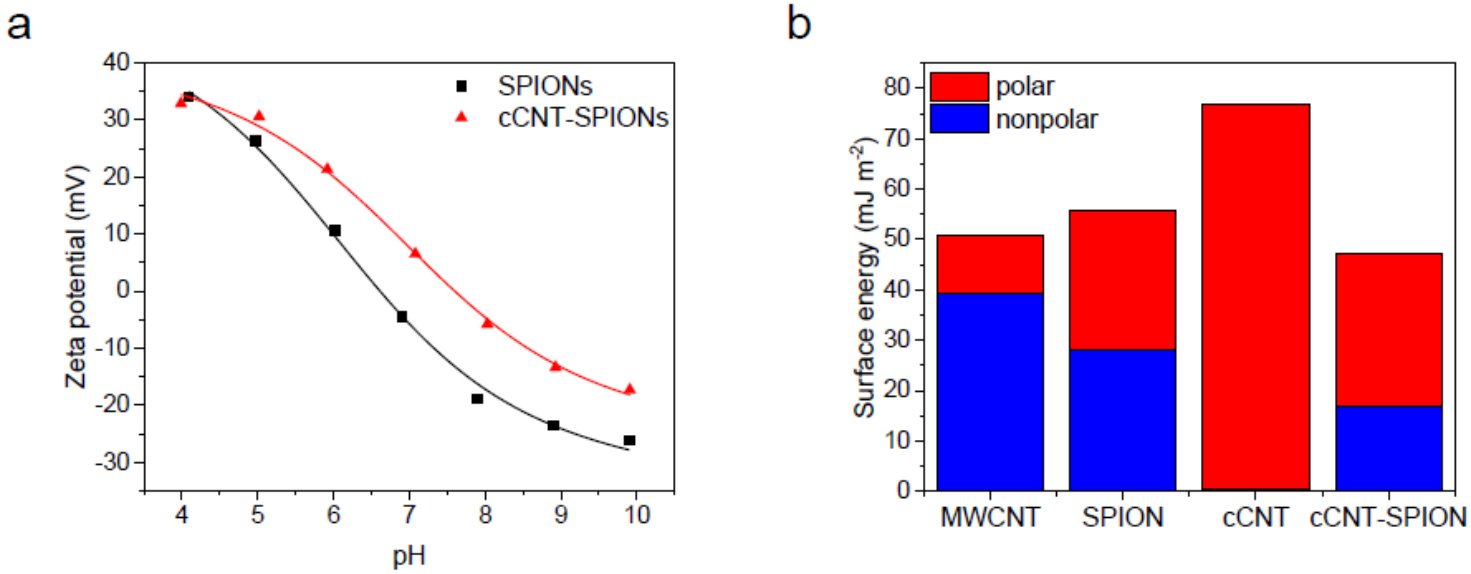

Figure 5

Zeta potential of SPIONs and cCNT-SPIONs from pH 4 to 10 a and surface free energy obtained from capillary rise experiments with the OWRK method b

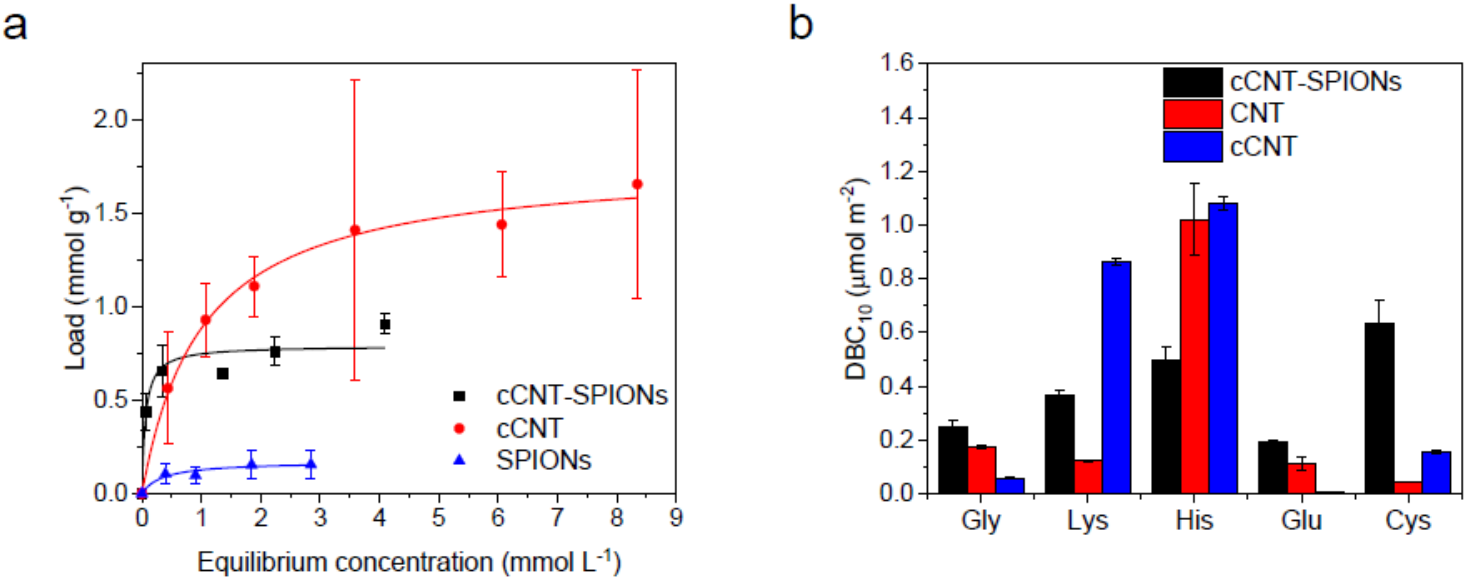

Figure 6

Static binding capacities of L-lysine with cCNTs, cCNT-SPIONs and SPIONs at pH 7.8 with 100 mM phosphate buffer a. Dynamic binding capacities at 10% of the breakthrough of cCNT-SPIONs, CNTs and cCNTs obtained from inverse chromatography experiments with different amino acids at pH 6 b.

Supplementary Files

This is a list of supplementary files associated with this preprint. Click to download.

- SupplementaryMaterialNRL.pdf